ORGANOMETALLICS

Article

pubs.acs.org/Organometallics

Terms of Use CC-BY

Bioinspired Hydrogenase Models: The Mixed-Valence Triiron Complex $[Fe_3(CO)_7(\mu\text{-edt})_2]$ and Phosphine Derivatives $[Fe_3(CO)_{7-x}(PPh_3)_x(\mu\text{-edt})_2]$ (x = 1, 2) and $[Fe_3(CO)_5(\kappa^2\text{-diphosphine})(\mu\text{-edt})_2]$ as Proton Reduction Catalysts

Ahibur Rahaman,[†,‡] Shishir Ghosh,[†,§] David G. Unwin,[§] Sucharita Basak-Modi,[§] Katherine B. Holt,*[,§] Shariff E. Kabir,*[,†] Ebbe Nordlander,[‡] Michael G. Richmond,[∥] and Graeme Hogarth*[,§,⊥]

[†]Department of Chemistry, Jahangirnagar University, Savar, Dhaka 1342, Bangladesh

[‡]Inorganic Chemistry Research Group, Chemical Physics, Center for Chemistry and Chemical Engineering, Lund University, P.O. Box 124, SE-22100 Lund, Sweden

[§]Department of Chemistry, University College London, 20 Gordon Street, London WC1H 0AJ, U.K.

[∥]Department of Chemistry, University of North Texas, 1155 Union Circle, Box 305070, Denton, Texas 76203, United States

[⊥]Department of Chemistry, King's College London, Britannia House, 7 Trinity Street, London SE1 1DB, U.K.

Supporting Information

ABSTRACT: The mixed-valence triiron complexes $[Fe_3(CO)_{7-x}(PPh_3)_x(\mu\text{-edt})_2]$ (x = 0–2; edt = SCH_2CH_2S) and $[Fe_3(CO)_5(\kappa^2\text{-diphosphine})(\mu\text{-edt})_2]$ (diphosphine = dppv, dppe, dppb, dppn) have been prepared and structurally characterized. All adopt an *anti* arrangement of the dithiolate bridges, and PPh_3 substitution occurs at the apical positions of the outer iron atoms, while the diphosphine complexes exist only in the dibasal form in both the solid state and solution. The carbonyl on the central iron atom is semibridging, and this leads to a rotated structure between the bridged diiron center. IR studies reveal that all complexes are inert to protonation by $HBF_4\cdot Et_2O$, but addition of acid to the pentacarbonyl complexes results in one-electron oxidation to yield the moderately stable cations $[Fe_3(CO)_5(PPh_3)_2(\mu\text{-edt})_2]^+$ and $[Fe_3(CO)_5(\kappa^2\text{-diphosphine})(\mu\text{-edt})_2]^+$, species which also result upon oxidation by $[Cp_2Fe][PF_6]$. The electrochemistry of the formally Fe(I)–Fe(II)–Fe(I) complexes has been investigated. Each undergoes a quasi-reversible oxidation, the potential of which is sensitive to phosphine substitution, generally occurring between 0.15 and 0.50 V, although $[Fe_3(CO)_5(PPh_3)_2(\mu\text{-edt})_2]$ is oxidized at −0.05 V. Reduction of all complexes is irreversible and is again sensitive to phosphine substitution, varying between −1.47 V for $[Fe_3(CO)_7(\mu\text{-edt})_2]$ and around −1.7 V for phosphine-substituted complexes. In their one-electron-reduced states, all complexes are catalysts for the reduction of protons to hydrogen, the catalytic overpotential being increased upon successive phosphine substitution. In comparison to the diiron complex $[Fe_2(CO)_6(\mu\text{-edt})]$, $[Fe_3(CO)_7(\mu\text{-edt})_2]$ catalyzes proton reduction at 0.36 V less negative potentials. Electronic structure calculations have been carried out in order to fully elucidate the nature of the oxidation and reduction processes. In all complexes, the HOMO comprises an iron–iron bonding orbital localized between the two iron atoms not ligated by the semibridging carbonyl, while the LUMO is highly delocalized in nature and is antibonding between both pairs of iron atoms but also contains an antibonding dithiolate interaction.

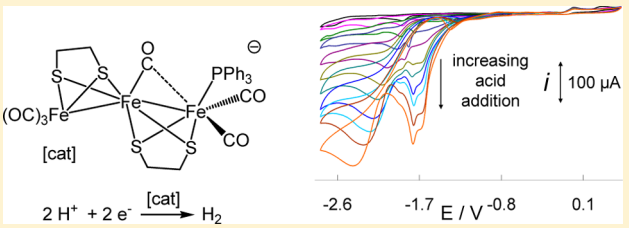

INTRODUCTION

Over the past decade there has been intense interest in the chemistry of dithiolate-bridged diiron complexes,[1−5] since they closely resemble the two-iron unit of the H-cluster active site of iron-only hydrogenases.[6−8] As a result of these studies important advances have been made in our understanding of how this enzyme site functions;[9−12] however, many challenges remain. Most notably, while it is relatively easy to prepare complexes which bear a close structural resemblance to the H-cluster site, the preparation of good functional models has not yet been achieved. Thus, while virtually all diiron(I) dithiolate-bridged complexes are able to act as catalysts for the reduction of protons to hydrogen under reducing conditions, they are generally characterized by high overpotentials and poor turnover numbers and frequencies.

In 2005, Pickett and co-workers reported the serendipitous isolation of the tetrairon cluster $[Fe_4(CO)_8\{\mu_3\text{-}(SCH_2)_3CMe\}_2]$ (**A**) formed upon reaction of Bosnich's thiol with $[Fe_3(CO)_{12}]$.[13] This is a rare example of a linear 66-electron cluster being characterized by three metal–metal bonds[14−19] and is formally a mixed-valence complex comprised

Received: July 15, 2013
Published: March 5, 2014

 © 2014 American Chemical Society dx.doi.org/10.1021/om400691q | *Organometallics* 2014, 33, 1356−1366

Scheme 1

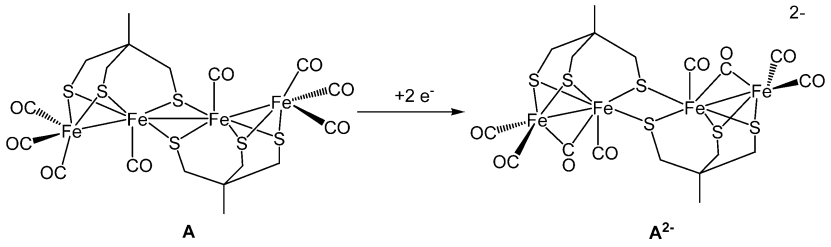

Scheme 2

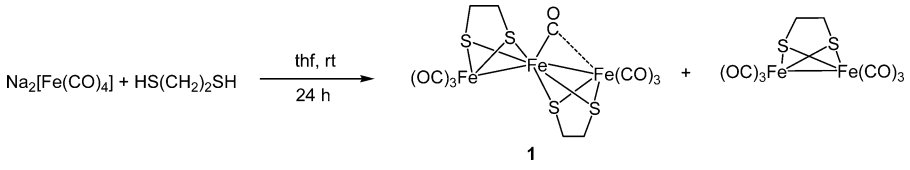

Scheme 3

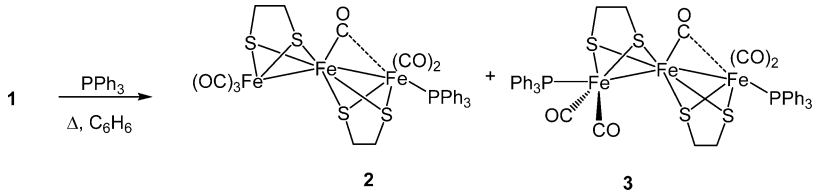

of a chain of Fe(I)−Fe(II)−Fe(II)−Fe(I) centers.[20] Importantly with respect to functional modeling of the hydrogenase active site, while the one-electron-reduction product $\mathbf{A}^-$ was shown to be only a moderate catalyst for proton reduction, addition of a second electron resulted in formation of $\mathbf{A}^{2-}$, which was shown to be an excellent electrocatalyst, dihydrogen elimination being at least 500 times greater than that found in related $[Fe_2(CO)_6(\mu\text{-dithiolate})]$ complexes.[13] Later detailed electrochemical and DFT studies shed some light onto the high activity of $\mathbf{A}^{2-}$.[20,21] Thus, it is proposed that upon addition of two electrons the central iron−iron bond of **A** is cleaved, which in turn leads to *rotation* of the iron tricarbonyl groups and formation of bridging carbonyls and vacant coordination sites, the latter being able to bind protons efficiently and thus leading to high electrocatalytic ability (Scheme 1).[20,21]

These results prompted us to consider other mixed-valence iron thiolate clusters as potential electrocatalysts for proton reduction. In an early paper on the synthesis of diiron dithiolate complexes, Huttner and co-workers reported that while reaction of $HS(CH_2)_nSH$ (n = 2, 3) with $[Fe_3(CO)_{12}]$ afforded predominantly the diiron complexes $[Fe_2(CO)_6\{\mu\text{-}S(CH_2)_nS\}]$, in both cases smaller amounts of the trinuclear materials $[Fe_3(CO)_7\{\mu\text{-}S(CH_2)_nS\}_2]$ could also be isolated.[22] No later reports detail these mixed-valence complexes, and consequently we were drawn to investigate them as possible electrocatalysts for proton reduction. Herein we describe our studies in this area which have focused on the ethanedithiolate (edt) complex $[Fe_3(CO)_7(\mu\text{-edt})_2]$ (**1**), some aspects of which have previously been communicated.[23]

RESULTS AND DISCUSSION

Synthesis $[Fe_3(CO)_7(\mu\text{-edt})_2]$ (1). Huttner and coworkers initially reported the preparation of $[Fe_3(CO)_7(\mu\text{-edt})_2]$ (**1**) in <1% yield from a 1:1 reaction between 1,2-ethanedithiol and $[Fe_3(CO)_{12}]$ in toluene at 70 °C, raising the yield to 5% upon doubling the amount of 1,2-ethanedithiol.[22] We were not able to reproduce this latter yield following Huttner's method, our best yield being less than 2%. In an attempt to prepare **1** in larger amounts, we reacted 2 equiv of Collman's reagent, $Na_2[Fe(CO)_4]$, with 1,2-ethanedithiol at room temperature in thf over 24 h. This resulted in isolation of **1** after chromatographic workup as a red solid in 5% yield, the major product (27%) being $[Fe_2(CO)_6(\mu\text{-edt})]$ (Scheme 2). While it is not clear to us why this method gives better results, it has been repeated many times and is fully reproducible. Characterization data are in accord with those reported earlier.[22] In the ^{1}H NMR spectrum, four broad high-field resonances were assigned to the methylene protons of the edt bridges. The ^{13}C NMR spectrum has not previously been reported. Singlets at 37.7 and 36.2 ppm are assigned to the edt bridges, while the low-field region consists of five singlets in a 1:2:1:1:2 ratio. That at 221.5 ppm is assigned to the carbonyl bound to the central iron atom, while the other resonances are attributed to apical (intensity 1) and basal (intensity 2) carbonyls bound to the other iron atoms. These observations show that the solid-state structure (see below) is maintained in solution. The IR spectrum shows a series of strong absorptions between 2073 and 1975 cm^{-1} together with a weak absorption at 1904 cm^{-1}, which we attribute to the carbonyl on the central iron atom. This latter assignment was subsequently corroborated by DFT calculations (see later), which revealed a semibridging ν(CO) band at 1899 cm^{-1} in excellent agreement with the experimental data.

Reactivity of $[Fe_3(CO)_7(\mu\text{-edt})_2]$ (1) toward PPh_3. Phosphine substitution has been extensively utilized in work on diiron hydrogenase biomimetics, primarily in order to increase the electron density on the metal center and thus facilitate proton binding.[24−31] Heating a benzene solution of **1** and PPh_3 resulted in the slow consumption of starting materials with concomitant formation of four new products identified

dx.doi.org/10.1021/om400691q | Organometallics 2014, 33, 1356−1366

after chromatographic separation. Two of these were the desired substituted triiron complexes $[Fe_3(CO)_6(PPh_3)(\mu\text{-edt})_2]$ (**2**) (23%) and $[Fe_3(CO)_5(PPh_3)_2(\mu\text{-edt})_2]$ (**3**) (12%) (Scheme 3). Yields of both were dependent upon the reaction time, and it was clear that they were formed sequentially. Two further products were also isolated, binuclear $[Fe_2(CO)_5(PPh_3)(\mu\text{-edt})]$ (22%)[38] and $Ph_3P{=}S$ (30%). Competition between carbonyl substitution and iron−iron bond scission is a recurring feature of reactions in **1** and $[Fe_3(CO)_7(\mu\text{-pdt})_2]$ with mono- and bidentate phosphines.[39] Characterization of the desired triiron complexes was relatively straightforward. In the IR spectrum of **2** the low-energy carbonyl absorption now appears at 1882 cm^{-1}, while in **3** it is seen at 1869 cm^{-1}. The energies of these semibridging $\nu(CO)$ bands compare well with the DFT computed values of 1886 and 1873 cm^{-1}. The $^{31}P\{^1H\}$ NMR spectrum of **2** shows two singlets at 65.0 and 52.7 ppm in an approximate 3:1 ratio, which we attribute to the coexistence of isomers. This is supported by the ^1H NMR spectrum, in which a doubling of the expected peaks is seen. The major isomer shows four clear methylene resonances between δ 2.5 and 1.0, each appearing as a pseudodoublet (J = ca. 7−8 Hz) consistent with monosubstitution. The $^{31}P\{^1H\}$ NMR spectrum of **3** consists of three singlets at 63.8, 61.5, and 53.1 ppm in an approximate 2.5:3.5:1 ratio, which we attribute to two isomers; the resonance at 61.5 ppm is attributed to overlapping singlets. The existence of only two isomers is easily surmised from the ^1H NMR spectrum, which shows two pairs of methylene resonances in an approximate 2.5:1 ratio.

Reactivity of $[Fe_3(CO)_7(\mu\text{-edt})_2]$ (1) toward Diphosphines. Addition of diphosphines to the diiron center of hydrogenase biomimetics has been extensively studied and leads to an increase in electron density at the center, thus promoting protonation, but also binding of the diphosphines in a chelating manner affords steric and electronic differentiation of the two iron atoms.[31−37] Heating **1** in benzene with a range of diphosphines led to the isolation after chromatography of two product types, namely the desired triiron complexes $[Fe_3(CO)_5(\kappa^2\text{-diphosphine})(\mu\text{-edt})_2]$ (**4**−**7**) (Scheme 4) together with the diiron species $[Fe_2(CO)_4(\kappa^2\text{-diphosphine})(\mu\text{-edt})]$ (diphosphine = dppv, dppe, dppb).[37,39] The latter result formally from diphosphine addition to the central iron atom followed by metal−metal bond scission. These complexes are more easily prepared upon addition of the same diphosphines to $[Fe_2(CO)_6(\mu\text{-edt})]$ and will be reported more fully elsewhere.[39]

Scheme 4

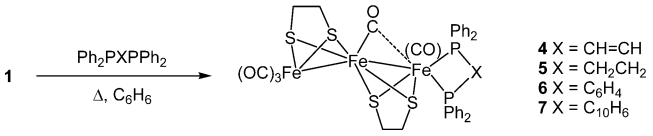

The triiron complexes **4**−**7** were isolated in moderate yields (20−40%) as air-stable red crystalline solids. They are readily characterized by their IR spectra, which show three absorption bands: a sharp and strong absorption at ca. 2025 cm^{-1}, a broad strong absorption at ca. 1950 cm^{-1}, and a weak absorption at ca. 1830 cm^{-1}. The last band shows that the semibridging carbonyl is still present. The ^1H NMR spectra are generally uninformative but are consistent with the proposed formulation. The $^{31}P(^1H)$ NMR spectra are more useful; in all cases, these consist only of a sharp singlet at room temperature, showing the existence of a single isomer. For example, the spectrum of $[Fe_3(CO)_5(\kappa^2\text{-}Ph_2PCH{=}CHPPh_2)(\mu\text{-edt})_2]$ (**4**) consists only of a singlet at 81.6 ppm and cooling to −60 °C in CD_2Cl_2 results in no significant broadening. Thus, we conclude that coordination of the diphosphine occurs exclusively in the basal positions of one of the outer iron atoms, a supposition that is supported both by crystallography and by DFT calculations (vide infra).

While this work was in progress, Schollhammer and coworkers reported the preparation of a diphosphine complex, $[Fe_3(CO)_5(\kappa^2\text{-diphosphine})(\mu\text{-pdt})]$ (diphosphine = 1,3,5,7-tetraphenyl-1,5-diaza-3,7-diphosphacyclooctane), related to **4**−**8** as a low-yield product from the reaction of $[Fe_2(CO)_6(\mu\text{-pdt})]$ with the diphosphine in refluxing toluene.[40] In light of the work described here, it seems probable that this results from the reaction of small amounts of $[Fe_3(CO)_7(\mu\text{-pdt})_2]$ in the diiron starting material.

Structural Studies. Crystallographic studies were carried out on **1**−**4**, the results of which are summarized in Figure 1 and Table 1. Data for **3** are relatively poor but nevertheless show clearly the sites of phosphine substitution and thus are included here. The diphosphine complex **4** contains a crystallographic plane of symmetry that includes the three iron atoms and the semibridging carbonyl.

All clusters contain an approximately linear triiron core (Fe(1)−Fe(2)−Fe(3) 151.50(6)−154.77(3)°) and an *anti* arrangement of dithiolate ligands. Iron−iron distances of 2.5385(8)−2.584(2) Å compare well with the Fe(I)−Fe(II) bond length of 2.543(5) Å found in $[Fe_4(CO)_8\{\mu_3\text{-}(SCH_2)_3CMe\}_2]$[13] but are shorter than the Fe(II)−Fe(II) contact of 2.651(9) Å in the same molecule. In **2** and **3** phosphine substitution occurs at the apical site(s) of the external Fe(I) centers lying approximately *trans* to the metal−metal bond (Fe−Fe−P 150.27(9)−154.11(8)°). In contrast, the diphosphine in **4** occupies basal sites at the iron center that is bound to the semibridging carbonyl and subtends a bite angle of 86.71(4)°. A feature of all complexes is the bending of the carbonyl bound to the Fe(II) center (Fe(2)−C−O 160.4(3)−168.2(8)°) (see below), while the Fe(2)−C bond distances of 1.75(1)−1.774(4) Å are somewhat shorter than those for the carbonyls bound to the Fe(I) centers, with the exception of the unique carbonyl at the Fe(CO)(diphosphine) center in **4** (Fe(1)−C(1) 1.750(4) Å). Again a similar but less pronounced effect is seen in $[Fe_4(CO)_8\{\mu_3\text{-}(SCH_2)_3CMe\}_2]$, where the Fe^{II}−C bond length is 1.771(3) Å.[13]

The structure of **1** is very similar to that of *anti*-$[Ru_3(CO)_7(\mu\text{-edt})_2]$ reported by Adams and Yamamoto.[41] Importantly, the bond angle at the central metal site of 151.52(3)° is virtually identical with those in **1**−**4**, while the central carbonyl is also bent (Ru(2)−C−O 166.4(8)°). This has been attributed to a semibridging interaction with a second ruthenium atom (Ru(1)−C 2.713(9) Å). Similar interactions are seen in **1**−**3**, with Fe(1)···C(4), Fe(1)···C(3), and Fe(3)···C(3) bond lengths of 2.576(4), 2.61(1), and 2.57(1) Å, respectively. In **4** this interaction is even shorter (Fe(1)···C(2) 2.433(4) Å), suggesting that the increase in electron density at the iron(I) center upon phosphine addition enhances the semibridging interaction. Formation of a semibridging carbonyl is believed to be a key feature of proton reduction by hydrogenase enzymes,[1−5] and a number of biomimetic Fe(I)−Fe(II) complexes contain this feature.[42−45]

dx.doi.org/10.1021/om400691q | *Organometallics* 2014, 33, 1356−1366

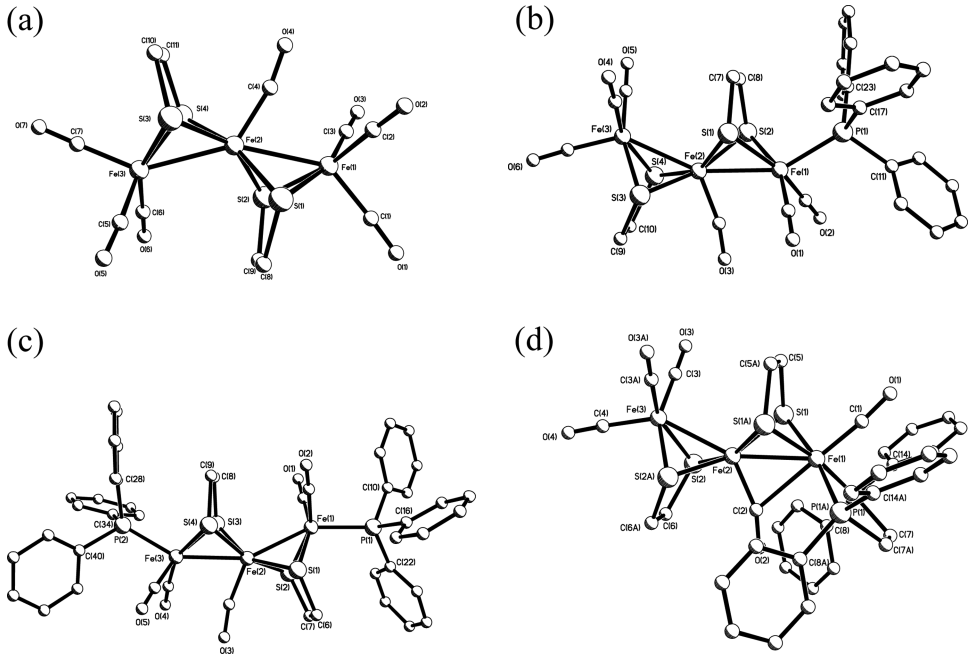

Figure 1. Molecular structures of (a) $[Fe_3(CO)_7(\mu\text{-edt})_2]$ (**1**), (b) $[Fe_3(CO)_6(PPh_3)(\mu\text{-edt})_2]$ (**2**), (c) $[Fe_3(CO)_5(PPh_3)_2(\mu\text{-edt})_2]$ (**3**), and (d) $[Fe_3(CO)_5(\kappa^2\text{-dppv})(\mu\text{-edt})_2]$ (**4**).

Table 1. Selected Bond Lengths (Å) and Angles (deg) for 1−4

	1	2	3	4
Fe(1)−Fe(2)	2.5385(8)	2.546(2)	2.547(2)	2.556(1)
Fe(2)−Fe(3)	2.5655(8)	2.584(2)	2.546(2)	2.543(1)
Fe(1)−P(1)		2.244(3)	2.250(3)	2.221(8)
Fe(3)−P(2)			2.251(3)	
Fe(1)−S(1)	2.263(1)	2.249(3)	2.249(3)	2.554(8)
Fe(1)−S(2)	2.252(1)	2.261(3)	2.257(3)	
Fe(2)−S(1)	2.241(1)	2.258(3)	2.226(3)	2.2533(8)
Fe(2)−S(2)	2.235(1)	2.256(3)	2.248(3)	2.2075(9)
Fe(2)−S(3)	2.215(1)	2.210(3)	2.239(3)	
Fe(2)−S(4)	2.216(1)	2.198(3)	2.269(3)	
Fe(3)−S(3)	2.238(1)	2.238(3)	2.270(3)	2.2534(9)
Fe(3)−S(4)	2.237(1)	2.238(3)	2.281(3)	
Fe(1)−Fe(2)−Fe(3)	151.74(3)	151.83(7)	151.50(6)	154.77(3)
Fe−S(1)−Fe	68.62(3)	68.79(8)	69.39(9)	69.08(3)
Fe−S(2)−Fe	68.90(3)	68.61(9)	68.87(8)	69.50(3)
Fe−S(3)−Fe	70.36(3)	71.05(9)	68.74(8)	
Fe−S(4)−Fe	70.37(4)	71.26(8)	68.05(8)	
Fe(2)−Fe(1)−P(1)		150.27(9)	154.11(8)	115.41(3)
Fe(2)−Fe(3)−P(2)			151.03(8)	
Fe(2)−C−O	167.6(4)	167.7(9)	168.2(8)	160.4(3)
Fe(2)−C	1.765(4)	1.76(1)	1.75(1)	1.774(4)
Fe(1)···C	2.576(4)	2.61(1)	2.57(1)	2.433(4)

Acid Addition and Chemical Oxidation. A key step in the electrocatalytic conversion of protons to hydrogen at the active center is the coordination of the proton(s). The hexacarbonyl complexes $[Fe_2(CO)_6(\mu\text{-dithiolate})]$ are protonated only when especially strong acids are used,[46] and thus phosphine substitution is typically employed in order to increase the proton-binding properties of binuclear models.[24−37,47,48] Before embarking on electrocatalytic studies, we therefore decided to investigate the reactions of **1**−**4** with acids. In no case did we find any evidence for the formation of a protonated species. Addition of a slight excess of $HBF_4{\cdot}Et_2O$ to a dichloromethane solutions of **1** resulted in no discernible change, while dark red **2** resulted in a slow lightening of the solution with concomitant growth of some new IR bands; however, this species showed limited stability and decomposed slowly. Addition of $HBF_4{\cdot}Et_2O$ to **3** in air resulted in a rapid lightening of the solution and the appearance of new IR bands at 2042 vs, 2021 m, and 1988 m cm^{-1}. Attempts to observe this compound by NMR spectroscopy were unsuccessful, and the excessively broadened spectrum was attributed to the generation of a paramagnetic species. Thus, we considered that the "protonation" product of **3** was rather an oxidation

dx.doi.org/10.1021/om400691q | *Organometallics* 2014, 33, 1356−1366

product. This was confirmed upon addition of 1 equiv of $[Cp_2Fe][PF_6]$ to a dichloromethane solution of **3**, which resulted in the generation of $[Fe_3(CO)_5(PPh_3)_2(\mu\text{-edt})_2][PF_6]$ ($[\mathbf{3}^+][PF_6]$), having an IR spectrum identical to that generated upon HBF_4 addition. The lack of a semibridging carbonyl band shows that some structural rearrangement has occurred upon oxidation. Unfortunately, we have not been able to obtain $\mathbf{3}^+$ in a pure state. Addition of $HBF_4{\cdot}Et_2O$ to **4** followed a similar course: an immediate lightening of the dark red solution with concomitant formation of a new species characterized by IR bands at 2071 vs, 2015 s, 1984 m, 1954 m, and 1908 w cm^{-1} with limited stability. As was the case for **3**, addition of $[Cp_2Fe][PF_6]$ led to the generation of an indistinguishable IR spectrum and for **5** and **6** similar changes were noted upon addition of $HBF_4{\cdot}Et_2O$.

Electronic Structure Calculations. In order to better understand the nature of the mixed valency and also in an attempt to interpret the electrochemical studies (see below), we have carried out a series of density functional calculations on **1**−**4**. For all four compounds the optimized structure was that seen crystallographically, suggesting that for **2**−**4** the observed phosphine substitution position(s) was the thermodynamic isomer. For related diiron complexes containing chelating diphosphines both apical−basal and dibasal isomers coexist in solution,[31−37] the relative energies being on the order of 0.5−1.5 kcal mol^{-1}. Using DFT we have calculated the energy difference between the observed dibasal form of **4** and its basal−apical isomer, the difference of 5.7 kcal mol^{-1} in favor of the dibasal isomer equating to $K_{eq} = 5.6 \times 10^{-5}$, in accord with our observation of a single isomer.

Phosphine substitution appears to have little impact on the nature of both the HOMO and LUMO (see the Supporting Information for full details), and thus only those for **1** are shown (Figure 2). The HOMO (Figure 2a) is best described as

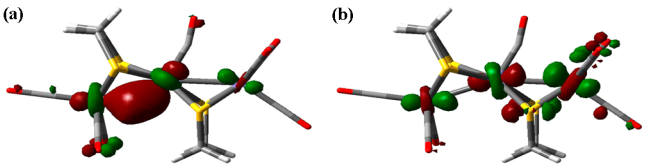

Figure 2. (a) HOMO and (b) LUMO of $[Fe_3(CO)_7(\mu\text{-edt})_2]$ (**1**). The contour plots are printed at an isovalue of 0.055.

an iron−iron bonding orbital that is localized on the pair of iron atoms not ligated by the semibridging carbonyl ligand, although there is a small antibonding component across the second iron−iron bond. This suggests that partial depopulation of this orbital (oxidation) should lead to an elongation of one of the metal−metal bonds and result in a significant loss of symmetry. In **2** and **4** the introduced phosphine ligand lies remote to the significant iron−iron bonding contribution in the HOMO, and hence one might expect that it plays little part in the nature of the oxidation process. In contrast to the HOMO, the LUMO (Figure 2b) is highly delocalized in nature. It is clearly antibonding about both iron−iron bonds and also displays an antibonding dithiolate interaction (in-phase lone pair) at the iron−iron vector ligated by the semibridging carbonyl. Consequently, a one-electron reduction might be expected to result in a slight elongation of both metal−metal bonds and perhaps also some elongation of some of the iron−sulfur bonds. It is noteworthy that the degree of the iron−sulfur antibonding interactions noted in the LUMOs of **2**−**4** is somewhat reduced in comparison to that in **1**, suggesting that the potential for sulfur−iron bond rupture upon reduction of the substituted clusters is reduced. The HOMO−LUMO gap is sensitive to the degree of phosphine substitution, decreasing from 3.01 eV in **1** to 2.95 and 2.80 eV in **2** and **3**, respectively, while the HOMO−LUMO gap in **4** of 3.28 eV is significantly larger.

Adams and Yamamoto have previously shown that *anti*-$[Ru_3(CO)_7(\mu\text{-edt})_2]$, formed upon addition of 1,2,5,6-tetrathioacyclooctane to $[Ru_3(CO)_{12}]$,[41] converts into the thermodynamically favored *syn* product upon heating (Scheme 5).

Scheme 5

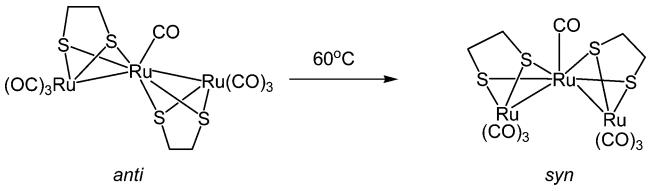

These isomers are structurally quite different, the most notable changes upon isomerization being (i) a significant lengthening of the ruthenium−ruthenium bonds of ca. 0.16 Å, (ii) a far more acute Ru−Ru−Ru bond angle of 73.55(2)°, and (iii) loss of the semibridging carbonyl interaction, while in the *syn* isomer both binuclear subunits contain nonrotated RuL_3 moieties. In *syn*-$[Ru_3(CO)_7(\mu\text{-edt})_2]$ the formally nonbonded Ru···Ru interaction is 3.4148(6) Å, which while being long could still be indicative of some direct interaction between these two atoms. DFT calculations (Figure 3) confirmed that for ruthenium the *syn* isomer lies 2.9 kcal mol^{-1} lower in enthalpy than the *anti* isomer. In contrast to the facile isomerization of *anti*-$[Ru_3(CO)_7(\mu\text{-edt})_2]$, heating a toluene solution of **1** resulted in no discernible change. A DFT calculation on the triiron system showed that the *syn* isomer is lower in enthalpy than the *anti* isomer, the difference of 1.1 kcal mol^{-1} being less than that found for the ruthenium complex. It is not clear why **1** does not undergo such an isomerization. It may be that the more radially contacted iron(I) centers cannot interact over the 3.53 Å computed for the internuclear Fe···Fe distance in the *syn* isomer, or it may simply be that the activation barrier is too high.

Electrochemical Studies. Cyclic voltammetry (CV) of **1**−**6** in dichloromethane under an argon atmosphere was carried out, important features being summarized in Table 2. CVs for **1**−**3** are shown in Figure 4. On scanning first to positive potentials, oxidation takes place at $E_{1/2}$ = 0.50 V for **1**, $E_{1/2}$ = 0.15 V for **2**, and $E_{1/2}$ = −0.05 V for **3**. The peak current for oxidation of **3** is significantly smaller than for **1** and **2**, suggesting that fewer electrons are transferred for this complex. Normalizing peak current by dividing by the square root of the scan rate reveals that twice as many electrons are transferred at low in comparison to high scan rates (Supporting Information); thus, we suggest a one-electron transfer at fast scan rates, tending to two electrons as the electrochemical time scale is increased. The limited stability of the oxidation product does not allow the number of electrons transferred to be determined using chronocoulometry experiments.

Of more importance in the context of proton reduction catalysis is the reduction behavior of the complexes. As expected, reduction potentials for **1**−**3** shift to more negative values with increased phosphine substitution (Figure 4). A

dx.doi.org/10.1021/om400691q | *Organometallics* 2014, 33, 1356−1366

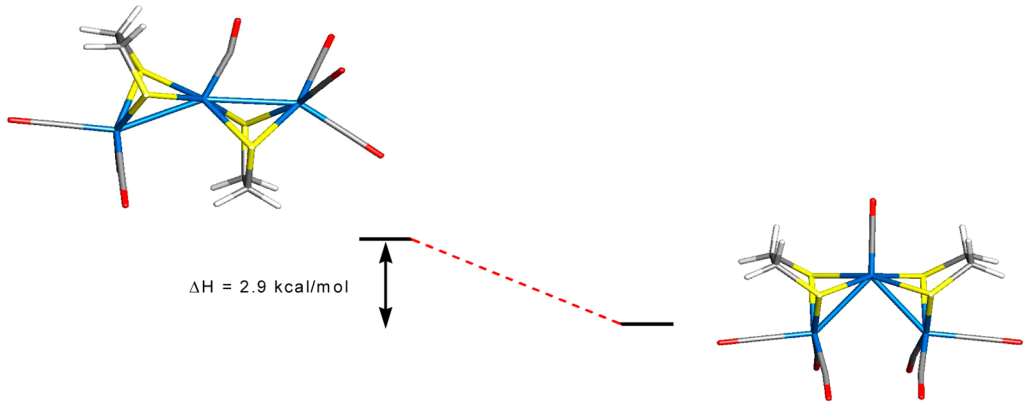

Figure 3. Geometry-optimized B3LYP structures of the *anti* (left) and *syn* (right) isomers and the ground-state enthalpy difference in the isomeric $[Ru_3(CO)_7(\mu\text{-edt})_2]$ clusters.

Table 2. Oxidation and Reduction Potentials of 1−6 in Dichloromethane

complex	peak potential (E_p) of first reduction (V)	$E_{1/2}$ of quasi-reversible oxidation (V)
$[Fe_3(CO)_7(\mu\text{-edt})_2]$ (**1**)	−1.47	0.50
$[Fe_3(CO)_6(PPh_3)(\mu\text{-edt})_2]$ (**2**)	−1.72	0.15
$[Fe_3(CO)_5(PPh_3)_2(\mu\text{-edt})_2]$ (**3**)	−1.82	−0.05
$[Fe_3(CO)_5(\kappa^2\text{-dppv})(\mu\text{-edt})_2]$ (**4**)	−1.74	0.29
$[Fe_3(CO)_5(\kappa^2\text{-dppe})(\mu\text{-edt})_2]$ (**5**)	−1.88	0.20
$[Fe_3(CO)_5(\kappa^2\text{-dppb})(\mu\text{-edt})_2]$ (**6**)	−1.68	0.36
$[Fe_3(CO)_5(\kappa^2\text{-dppv})(\mu\text{-edt})_2]$ (**4**)[a]	−1.89	0.00

[a]In MeCN.

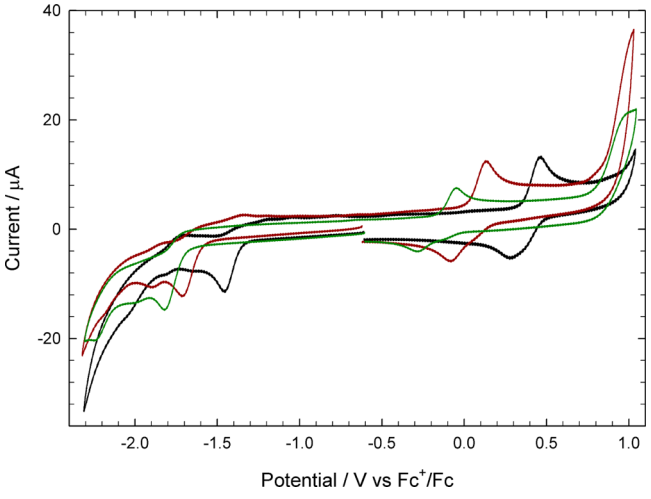

Figure 4. CVs of 0.5 mM **1** (black), **2** (brown), and **3** (green) in 0.1 M $TBAPF_6$ in dichloromethane under an Ar atmosphere, at a scan rate of 0.1 V s^{-1}.

comparison of the reduction peak currents with those for oxidation suggests that the reduction tends toward a two-electron process. Consistent with electronic structure calculations, we find $|E_p^{red} - E_p^{ox}|$ is sensitive to the degree of substitution. For **1**, the difference is 1.97 V, for **2** 1.87 V, and for **3** 1.77 V; the calculated HOMO−LUMO gaps are 3.01, 2.95, and 2.80 eV for **1**−**3**, respectively (vide supra). For all complexes reduction is irreversible at 0.1 V s^{-1}, indicative of significant structural change upon electron transfer. As the LUMO in each case is a delocalized antibonding orbital distributed over the three metal centers, it was anticipated that gain of an electron might lead simply to metal−metal bond elongation rather than a major structural change. However, a component of the LUMO is attributed to an iron−sulfur antibonding interaction, which could lead to iron−sulfur bond scission upon occupation. This structural change may allow uptake of a second electron at the same or less negative potential,[49] and thus an overall two-electron reduction process is noted. Repeating the voltammetry in CO-saturated solution does not improve the reversibility, indicating that CO ligand loss is not the major mechanism of decomposition (Supporting Information).

CVs for diphosphine derivatives **4**−**6** in dichloromethane were similar to those for **1**−**3.** As shown in Table 2 oxidation potentials vary only slightly upon changing the diphosphine ligand. This suggests that the electron that is removed is not localized on the substituted iron center, an observation in accord with the electronic structure calculations, which show the HOMO is delocalized over all three iron atoms. Complexes **4**−**6** show an irreversible reduction between −1.68 and −1.88 V, a potential range comparable with that of **2** and **3**, and the reduction is irreversible at all scan rates.

Electrocatalytic Studies. The reduction behavior of the complexes in the presence of protons was investigated in the presence of the strong acid HBF_4. For **1**−**3** in dichloromethane the principal catalytic response is observed at approximately the potential of the first reduction, at −1.5 V for **1**, −1.8 V for **2**, and −1.95 V for **3** (with 10 equiv of acid). The CVs of **2** with sequential addition of molar acid equivalents are presented in Figure 5, along with a plot of limiting catalytic current vs acid concentration for **1** and **2**. Although the catalytic activity of **2** takes place at more negative potentials as a consequence of its reduction potential, the catalytic peak currents obtained are higher than for unsubstituted **1**. Simulations reveal this is a consequence of the higher basicity of $\mathbf{2}^-$ and hence its more rapid protonation (Supporting Information). In excess acid some reduction currents are noted at potentials less negative than for the primary catalytic process, starting at −1.1 V. This suggests that a small quantity of neutral **2** may be protonated to form $\mathbf{2H}^+$, which can undergo reduction at much reduced overpotentials. The small magnitude of these currents confirms that protonation of **2** is sluggish and $\mathbf{2H}^+$ is a minority species. Further catalytic peaks are observed at ca. −2.0 and −2.3 V. The process at −2.0 V occurs at the potential at which a small reduction peak is noted for **2** in the absence of acid (Figure 4).

dx.doi.org/10.1021/om400691q | *Organometallics* 2014, 33, 1356−1366

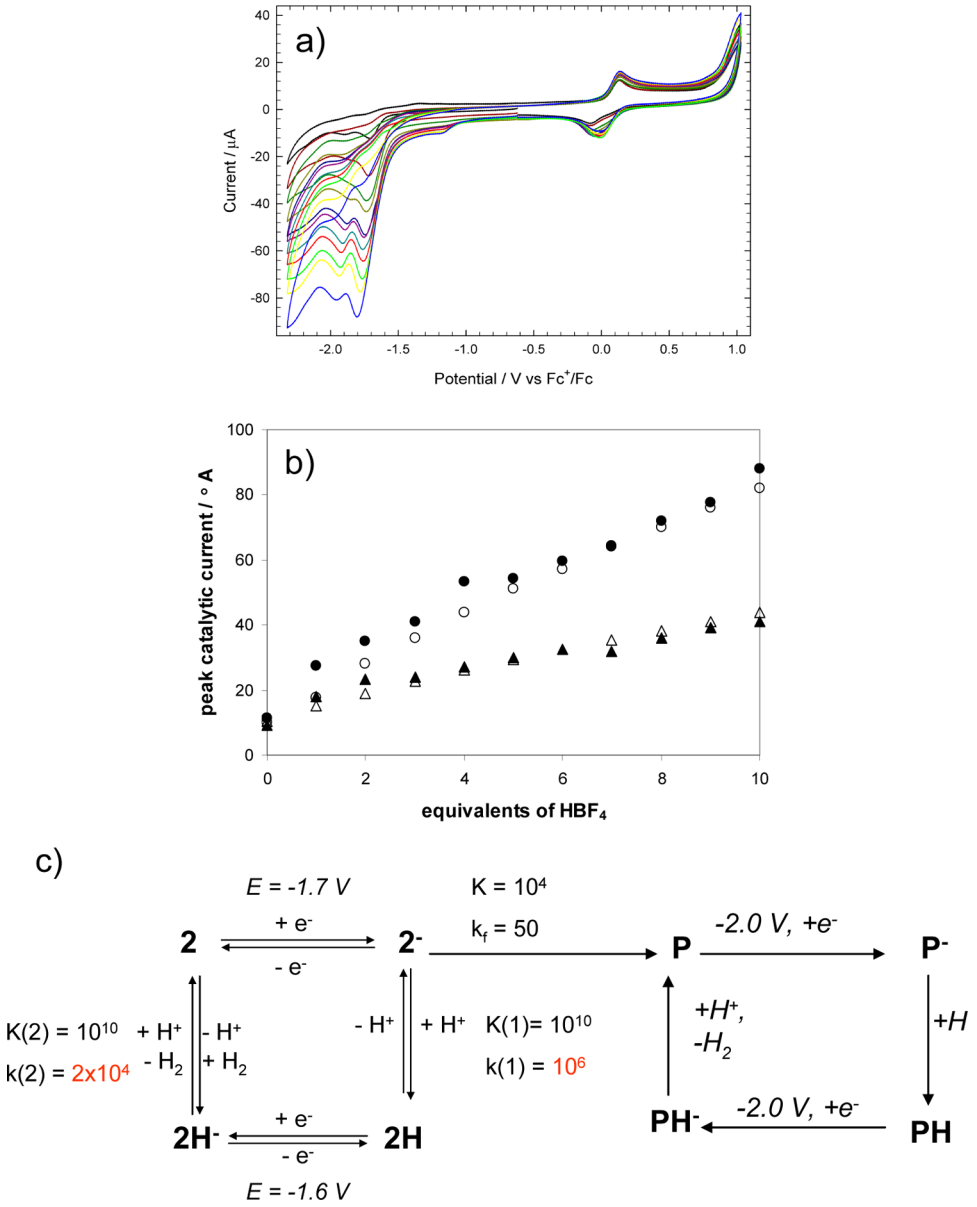

Figure 5. (a) CV of 0.5 mM **2** in 0.1 M $TBAPF_6$ in dichloromethane under Ar at a scan rate of 0.1 V s^{-1}. The black trace indicates the neutral complex only, and then HBF_4 is added in 0.5 mM increments. (b) Plot of experimental limiting catalytic current against molar equivalents of HBF_4 added for **1** (black triangles) and **2** (black circles) and simulated limiting catalytic currents for **1** (open triangles) and **2** (open circles) from DigiSim (see the Supporting Information). (c) Suggested ECEC mechanism of H^+ reduction with **2** and catalytic process at −2.0 V attributed to the decomposition product **P**. Parameters are described further in the Supporting Information. Values in red denote parameters that differ between **1** and **2**.

We attribute this peak to a decomposition product (**P3**) of 2^- (or 2^{2-}), resulting from scission of an Fe−S bond (vide supra). Hence, the catalytic response at the same potential is likely due to proton reduction associated with **P**. A suggested catalytic scheme is presented in Figure 5c. The peak at −2.3 V may be attributed to further reduction products, but direct reduction of the acid at the electrode also occurs in this potential region, making interpretation difficult.

We find catalytic currents for **2** are marginally higher than for **3**, indicating that further PPh_3 substitution does not result in faster proton reduction catalysis. This may be a result of slower protonation for 3^- than for 2^-, but if so this must be due to steric rather than electronic effects. The bulky PPh_3 group may prevent ready access for the proton to the Fe−Fe bond, or steric interactions between the edt bridge and the PPh_3 may prevent elongation of the Fe−Fe bond to accommodate a bridging hydride. Alternatively, this may be a consequence of the stability inferred on the **3H** catalytic intermediate species by the bulky phosphine ligands. For example, the species $[(\mu\text{-}H)Fe_2(pdt)(CO)_2(dppv)_2]$ has sufficient stability to be isolated, due to the basicity and steric bulk of phosphines.[50] Both computational[51] and experimental studies[50] suggest that this bridging hydride is a spectator, rather than an intermediate, in hydrogen evolution catalysis, although the exact mechanisms are unclear. It may be that a similar mechanism takes place for **3** and the rate-limiting step is not initial protonation of 3^- but subsequent steps involving the **3H** intermediate. For **2** we observe that the limiting current maintains a linear relationship with acid addition up to 10 equiv (Figure 5b), suggesting that under these conditions the rate-limiting step is acid dependent.

dx.doi.org/10.1021/om400691q | *Organometallics* 2014, 33, 1356−1366

Thus, in this regime it appears that one of the protonation steps, rather than H_2 elimination, is rate limiting. Further studies, including determination of scan rate dependence and the use of acids of different pK_a values would be required to further understand this mechanism and the difference in behavior of **2** and **3**.

In dichloromethane, sequential addition of HBF_4 to **4**–**6** results in irreproducible CVs, suggesting that the complexes are unstable under these conditions; thus, we are unable to provide a direct comparison of the influence of asymmetric substitution on the protonation or catalytic behavior of these complexes.

CONCLUDING REMARKS

Since it has been suggested that a rotated structure encompassing a semibridging carbonyl is essential for effective catalytic activity in hydrogenase biomimetic molecules, various synthetic routes have been explored to produce such a structure. Here we report the electrochemical and electrocatalytic activity of triiron complexes with this structural feature in their neutral form. In comparison to their diiron analogues the complexes are catalytic at decreased overpotential; for example, electrocatalytic proton reduction by $[Fe_3(CO)_7(\mu\text{-edt})_2]$ (**1**) takes place at 0.36 V less negative potentials than that when $[Fe_2(CO)_6(\mu\text{-edt})]$ is the catalyst. Substitution with PPh_3 or diphosphines does not increase the basicity of the complexes sufficiently to allow significant protonation of the neutral molecule in dichloromethane. The first step in the catalytic cycle is therefore reduction of the complex in an EC-initiated mechanism. Phosphines push the catalytic response to more negative potentials; however, the payoff is that higher catalytic currents can be achieved, as the rate-limiting step is protonation of the anion.

Recently a number of other groups have utilized triiron clusters as proton reduction catalysts,[52−55] most notably the bicapped 50-electron cluster $[Fe_3(\mu_3\text{-S})_2(CO)_9]$.[52,53,55] Linear triiron complexes **1**–**6** are considerably less stable to one-electron reduction than $[Fe_3(\mu_3\text{-S})_2(CO)_9]$, which undergoes a reversible one-electron reduction on the voltammetric time scale, and the monoanionic product has been detected spectroscopically,[53] although it is not stable enough to isolate with bulk electrolysis due to CO ligand loss.[52] On addition of a second electron at more negative potential $[Fe_3(\mu_3\text{-S})_2(CO)_9]^{2-}$ undergoes a rapid structural rearrangement with proposed Fe–S bond scission and formation of a bridging carbonyl across one iron–iron bond.[53] $[Fe_3(\mu_3\text{-S})_2(CO)_9]$ undergoes proton reduction catalysis via an ECEC mechanism at the potential of the first reduction, in a mechanism similar to that proposed for **2**. Catalytic processes at more negative potentials were attributed to the carbonyl-loss decomposition product of the monoanion and further reduction and protonation of the $[H_2Fe_3(\mu_3\text{-S})_2(CO)_9]$ intermediate from the primary catalytic cycle. The linear complexes described herein have reduction behavior very different from that of $[Fe_3(\mu_3\text{-S})_2(CO)_9]$, exhibiting irreversible reduction even at fast voltammetric scan rates. Reversibility is not improved in CO-saturated solutions, indicating that ligand loss is not a primary decomposition pathway. Electron uptake for **1**–**6** appears to be a two-electron process in the absence of acid, and as for $[Fe_3(\mu_3\text{-S})_2(CO)_9]$, we suggest that iron–sulfur bond rupture takes place. The linear complexes do not have the stability conferred by the cyclic structure; therefore, fragmentation into diiron and monoiron is a likely result.

Although they are not structural models for the hydrogenase enzyme active site, the triiron complexes described here have several features which make them potential functional models. The enzyme operates via the $Fe^{II}Fe^{I}$ oxidation states, as do the triiron complexes, while in contrast, most hydrogenase mimics operate via the $Fe^{I}Fe^{0}$ oxidation states. Further, the presence of the third iron center results in a HOMO–LUMO gap smaller than that for analogous diiron species The difference in potential between the first oxidation and first reduction of neutral **1** is 1.97 V, in contrast to 2.70 V for $[Fe_2(CO)_6(\mu\text{-edt})]$.[23] Similarly, the values are 1.87 V for **2**, in comparison to 2.60 V for $[Fe_2(CO)_5(PPh_3)(\mu\text{-edt})]$, and 1.77 V for **3**, in comparison to 2.45 V for $[Fe_2(CO)_4(PPh_3)_2(\mu\text{-edt})]$ (for experiments carried out under the same conditions).[23] In the enzyme the catalysis of proton reduction and hydrogen oxidation takes place reversibly and is close to the thermodynamic potential; thus, the difference in energy between the HOMO and LUMO must be very small. By designing biomimetics with a smaller HOMO–LUMO gap, we can hope to come closer to the catalytic performance of the enzyme. Unfortunately, the instability of the reduced forms of the complexes described here negates their use as viable proton reduction catalysts. Nevertheless, this work points toward the potential of small low-valent molecular clusters, especially those with mixed-valence states, to act as proton reduction catalysts.

EXPERIMENTAL SECTION

General Procedures and Starting Materials. Unless otherwise noted, all reactions were carried out under a nitrogen atmosphere using standard Schlenk techniques. Reagent-grade solvents were dried using appropriate drying agents and distilled prior to use by standard methods. Infrared spectra were recorded on a Shimadzu FTIR 8101 spectrophotometer. NMR spectra were recorded on a Bruker DPX 400 instrument. Mass spectra were recorded on a Varian Mat 312 mass spectrometer. Elemental analyses were performed by Microanalytical Laboratories, University College London. Collman's reagent and phosphines were purchased from Strem Chemical Inc. and used without further purification.

Preparation of $[Fe_3(CO)_7(\mu\text{-edt})_2]$ (1). To a suspension of $Na_2[Fe(CO)_4]$ (*ca.* 2.183 g, 10.20 mmol) in thf (30 mL) was added dropwise a solution of 1,2-ethanedithiol (0.479 g, 5.10 mmol) in thf (30 mL). After the mixture was stirred for 24 h at room temperature, the solvent was removed in vacuo and the residue extracted with hexane and filtered on Kieselguhr. The filtrate was concentrated under reduced pressure to give an orange gum, which was chromatographed by TLC on silica gel. Elution with hexane developed two bands. The faster-moving orange band gave $[Fe_2(CO)_6(\mu\text{-edt})]$ (512 mg, 27%) as red crystals, while the slower-moving band afforded $[Fe_3(CO)_7(\mu\text{-edt})_2]$ (**1**; 90 mg, 5%) as deep red crystals after recrystallization from hexane/CH_2Cl_2 at 4 °C. IR (ν(CO), CH_2Cl_2): 2073 s, 2040 vs, 2008 s, 1974 s, 1904 w cm^{-1}. ^{1}H NMR (CD_2Cl_2): 2.59 (br, 2H), 2.34 (br, 2H), 1.30 (br, 2H), 0.88 (br, 2H). $^{13}C\{^1H\}$ NMR (CD_2Cl_2): 221.5 (s, 1CO), 211.6 (s, 2CO), 207.3 (s, 1CO), 206.7 (s, 1CO), 206.0 (s, 2CO), 37.8 (s, CH_2), 36.2 (s, CH_2).

Preparation of $[Fe_3(CO)_6(PPh_3)(\mu\text{-edt})_2]$ (2) and $[Fe_3(CO)_5(PPh_3)_2(\mu\text{-edt})_2]$ (3). A benzene solution (20 mL) of **1** (75 mg, 0.137 mmol) and PPh_3 (36 mg, 0.137 mmol) was heated to reflux for 15 h. The solvent was removed under reduced pressure and the residue chromatographed by TLC on silica gel. Elution with hexane/CH_2Cl_2 (v/v 9/1) developed six bands. The first band was unreacted **1** (trace). The second to fifth bands afforded the following compounds in order of elution: $[Fe_2(CO)_5(PPh_3)(\mu\text{-edt})]$ (18 mg, 22%) as red crystals, $[Fe_3(CO)_6(PPh_3)(\mu\text{-edt})_2]$ (**2**; 25 mg, 23%) as orange crystals, $[Fe_3(CO)_5(PPh_3)_2(\mu\text{-edt})_2]$ (**3**; 16 mg, 12%) as red crystals, and Ph_3PS (15 mg, 30%) as white crystals after recrystallization from hexane/CH_2Cl_2 at −20 °C. Spectral data for **2** are as follows. Anal. Calcd for $C_{28}H_{23}Fe_3O_6PS_4$: C, 42.99; H, 2.96.

dx.doi.org/10.1021/om400691q | *Organometallics* 2014, 33, 1356−1366

Table 3. Crystallographic Data and Structure Refinement Details for 1−4

	1	2	3	4
empirical formula	$C_{11}H_8O_7Fe_3S_4$	$C_{28}H_{23}O_6Fe_3S_4P$	$C_{50}H_{38}O_{5.50}Fe_3S_4P_2$	$C_{35}H_{30}O_5Fe_3S_4P_2$
formula wt	547.96	782.22	1084.53	888.32
temp (K)	150(2)	150(2)	150(2)	150(2)
wavelength (Å)	0.71073	0.71073	0.71073	0.71073
cryst syst	triclinic	triclinic	orthorhombic	orthorhombic
space group	$P\bar{1}$	$P\bar{1}$	$C2/c$	$Pnma$
a (Å)	6.423(1)	8.799(5)	25.52(2)	29.939(7)
b (Å)	8.291(2)	11.268(6)	13.484(9)	17.775(5)
c (Å)	18.331(4)	16.543(9)	30.21(2)	8.513(2)
α (deg)	77.541(3)	90.571(7)	90	90
β (deg)	83.384(3)	90.499(1)	83.813(3)	90
γ (deg)	68.854(3)	109.469(8)	90	90
V (Å^3)	888.2(3)	1546.2(1)	10360(1)	3622.4(2)
Z	2	2	8	4
D_{calc} (Mg m^{-3})	2.0499	1.680	1.391	1.629
μ(Mo Kα) (mm^{-1})	2.918	1.751	1.096	1.546
F(000)	544	792	4432	1808
cryst color	red	orange	red	orange
cryst size (mm)	0.14 × 0.14 × 0.03	0.26 × 0.10 × 0.03	0.22 × 0.10 × 0.05	0.40 × 0.34 × 0.03
θ range (deg)	1.14−28.28	1.92−28.50	2.22−28.31	2.65−28.32
limiting indices	$-8 \le h \ge 8$	$-11 \le h \ge 11$	$-32 \le h \ge 33$	$-30 \le h \ge 31$
	$-10 \le k \ge 10$	$-14 \le k \ge 14$	$-17 \le k \ge 17$	$-23 \le k \ge 23$
	$-13 \le l \ge 24$	$-21 \le l \ge 20$	$-39 \le l \ge 39$	$-11 \le l \ge 10$
structure solution	Patterson	direct methods	direct methods	direct methods
no. of rflns collected	7497	12 859	41 674	28 927
no. of indep rflns (R_{int})	3970 (0.0333)	6918 (0.0526)	12131 (0.2646)	4433 (0.0695)
max, min transmission	0.9176, 0.6855	0.9493, 0.6588	0.9472, 0.7945	0.9551, 0.5767
no. of data/restraints/params	3970/0/226	6918/0/379	12131/0/581	4433/0/235
goodness of fit on F^2	1.051	1.052	0.960	0.906
final R indices ($I > 2\sigma(I)$)				
R1	0.0417	0.0943	0.1027	0.0396
wR2	0.1248	0.2600	0.2069	0.0854
R indices (all data)				
R1	0.0480	0.1181	0.2394	0.0661
wR2	0.1411	0.2787	0.2551	0.0903
largest diff peak, hole (e Å^{-3})	1.362, −0.649	1.045, −1.726	1.051, −0.631	1.430, −0.608

Found: C, 43.44; H, 3.07. IR (ν(CO), CH_2Cl_2): 2035 s, 2012 vs, 1963 vs, 1882 w cm^{-1}. ^{1}H NMR ($CDCl_3$): both isomers, δ 7.65 (m, 4H), 7.58 (m, 2H), 7.44 (m, 9H), 2.49 (m, 2H), 2.18 (m, 2H), 1.81 (m, 2H), 1.04 (m, 2H). ^{31}P{^{1}H} NMR ($CDCl_3$): major isomer, δ 65.0 (s); minor isomer, δ 52.7 (s). Spectral data for **3** are as follows. Anal. Calcd for $C_{45}H_{38}Fe_3O_5P_2S_4$: C, 53.17; H, 3.77. Found: C, 53.69; H, 3.91. IR (ν(CO), CH_2Cl_2): 2008 s, 1965 vs, 1953 sh, 1912 m, 1869 w cm^{-1}. ^{1}H NMR ($CDCl_3$): δ 7.66 (m, 10H), 7.39 (m, 20H), 1.98 (m, 4H), 1.01 (m, 2H), 0.77 (m, 2H). ^{31}P{^{1}H} NMR ($CDCl_3$): δ 63.8 (s), 61.5 (s), 53.1 (s).

Preparation of [$Fe_3(CO)_5(\kappa^2$-dppv)(μ-edt)$_2$] (4). A benzene solution (20 mL) of **1** (40 mg, 0.072 mmol) and *cis*-$Ph_2PCH{=}CHPPh_2$ (dppv; 29 mg, 0.073 mmol) was heated to reflux for 5 h. The solvent was removed under reduced pressure and the residue chromatographed by TLC on silica gel. Elution with hexane/CH_2Cl_2 (v/v 4/1) gave three bands. The first band was unreacted **1** (2 mg) (trace). The second band gave only a trace amount of product insufficient for characterization, and the third band gave [$Fe_3(CO)_5(\kappa^2$-dppv)(μ-edt)$_2$] (**4**; 23 mg, 37%) as red crystals, after recrystallization from hexane/CH_2Cl_2 at −20 °C. Spectral data for **4** are as follows. Anal. Calcd for $C_{35}H_{30}Fe_3O_5P_2S_4$: C, 47.29; H, 3.40. Found: C, 47.41; H, 3.49. IR (ν(CO), CH_2Cl_2): 2024 vs, 1951 s, 1942 s, 1830 w cm^{-1}. ^{1}H NMR ($CDCl_3$): δ 8.44−8.30 (m, 2H, CH=CH), 7.70−7.28 (m, 20H, Ph) 2.65 (d, J 8.0, 2H, CH_2), 2.51 (d, J 8.0, 2H, CH_2), 1.88 (m, 2H, CH_2), 1.74 (m, 2H, CH_2). ^{31}P{^{1}H} NMR ($CDCl_3$): δ 81.6 (s).

Preparation of [$Fe_3(CO)_5(\kappa^2$-dppe)(μ-edt)$_2$] (5). A benzene solution (20 mL) of **1** (40 mg, 0.072 mmol) and $Ph_2PCH_2CH_2PPh_2$ (dppe; 29 mg, 0.072 mmol) was heated to reflux for 4 h. The solvent was removed under reduced pressure, and the residue chromatographed by TLC on silica gel. Elution with hexane/CH_2Cl_2 (v/v 4/1) gave three bands. The first band was unreacted **1** (3 mg; trace). The second band afforded [$Fe_2(CO)_4(\mu$-edt)(κ^2-dppe)] (8 mg, 17%), and the third band gave [$Fe_3(CO)_5(\kappa^2$-dppe)(μ-edt)$_2$] (**5**; 20 mg, 33%) as red crystals, after recrystallization from hexane/CH_2Cl_2 at −20 °C. Spectral data for **5** are as follows. Anal. Calcd for $C_{35}H_{32}Fe_3O_5P_2S_4$: C, 47.19; H, 3.62. Found: C, 47.37; H, 3.69. IR (ν(CO), CH_2Cl_2): 2024 vs, 1951 m, 1830 w cm^{-1}. ^{1}H NMR ($CDCl_3$): δ 7.44−7.33 (m, 20H, Ph), 2.36−2.35 (m, 4H, CH_2), 2.29−2.27 (m, 4H, CH_2), 1.81−1.79 (m, 4H, CH_2). ^{31}P{^{1}H} NMR ($CDCl_3$): δ 71.0. ES-MS: m/z 913 [M^+ + Na] (calcd 913), 885 [M^+ + Na − CO] (calcd 885).

Preparation of [$Fe_3(CO)_5(\kappa^2$-dppb)(μ-edt)$_2$] (6). A benzene solution (20 mL) of **1** (40 mg, 0.072 mmol) and 1,2-$Ph_2PC_6H_4PPh_2$ (dppb; 33 mg, 0.073 mmol) was heated to reflux for 3 h. The solvent was removed under reduced pressure and the residue chromatographed by TLC on silica gel. Elution with hexane/CH_2Cl_2 (v/v 4/1) gave three bands. The first band was unreacted **1** (2 mg; trace). The second band gave a trace amount of [$Fe_2(CO)_4(\kappa^2$-dppb)(μ-edt)], and the third band gave [$Fe_3(CO)_5(\kappa^2$-dppb)(μ-edt)$_2$] (**6**; 22 mg, 34%) as red crystals, after recrystallization from hexane/CH_2Cl_2 at −20 °C. Spectral data for **6** are as follows. Anal. Calcd for $C_{39}H_{32}Fe_3O_5P_2S_4$: C, 49.89; H, 3.43. Found: C, 49.95; H, 3.50. IR (ν(CO), CH_2Cl_2): 2024

dx.doi.org/10.1021/om400691q | Organometallics 2014, 33, 1356−1366

vs, 1951 s, 1815 w cm^{-1}. ^1H NMR ($CDCl_3$): δ 7.79−7.62 (m, 4H, Ph), 7.35−7.19 (m, 20H, Ph), 2.52−2.32 (m, 4H, CH_2), 1.85−1.83 (m, 4H, CH_2). $^{31}P\{^1H\}$ NMR ($CDCl_3$): δ 84.0 (s, P). ES-MS: m/z 938 [M^+] (calcd 938), 960 [M^+ + Na] (calcd 961),

Preparation of $[Fe_3(CO)_5(\kappa^2\text{-dppn})(\mu\text{-edt})_2]$ (7). A benzene solution (20 mL) of **1** (50 mg, 0.091 mmol) and bis-(diphenylphosphino)naphthalene (dppn; 45 mg, 0.091 mmol) was heated to reflux for 12 h. The solvent was removed under reduced pressure and the residue chromatographed on silica gel. Elution with hexane/CH_2Cl_2 (v/v 4/1) gave three bands. The first band was unreacted dppn (trace). The second and third bands gave respectively $[Fe_2(CO)_4(\mu\text{-edt})(\kappa^2\text{-dppn})]$ (25 mg, 33%) and $[Fe_3(CO)_5(\mu\text{-edt})_2(\kappa^2\text{-dppn})]$ (7; 22 mg, 24%) as deep red crystals, after recrystallization from hexane/CH_2Cl_2 at −20 °C. Spectral data for **7** are as follows. Anal. Calcd for $C_{43}H_{34}Fe_3O_5P_2S_4$: C, 52.24; H, 3.47. Found: C, 52.72; H, 3.57. IR (ν(CO), CH_2Cl_2): 2024 vs, 1951 vs, 1817 w cm^{-1}. ^1H NMR ($CDCl_3$): δ 8.11−7.93 (m, 6H, Ph), 7.64−7.34 (m, 10H, Ph), 7.14−6.82 (m, 10H, Ph), 2.59−2.57 (m, 2H, CH_2), 2.33−2.31 (m, 2H, CH_2), 2.22−2.20 (m, 2H, CH_2), 2.02−2.06 (m, 2H, CH_2). $^{31}P\{^1H\}$ NMR ($CDCl_3$): δ 60.3 (s).

IR Studies of Addition of $HBF_4{\cdot}Et_2O$ and $[Cp_2Fe][PF_6]$ to 1−6. All reactions were carried out in a similar manner and monitored by IR spectroscopy.

Protonation. A CH_2Cl_2 solution (ca. 1 mL) of **1**−**6** was made by dissolving 2.5 × 10^{-3} mmol of the complex under study, and 2 molar equiv of $HBF_4{\cdot}Et_2O$ (0.680 μL) was added to this solution in the presence of air. The resultant acid-containing solution was immediately transferred to an IR cell and monitored over time. For **1** no discernible change in the IR spectrum was noted. For **2** a slow (ca. 1 h) lightening of the solution lead to the generation of new IR bands at 2103 m, 2062 sh, 2039 vs, 2001 s, and 1955 w cm^{-1}, but over this time there was also substantial decomposition. For **3** a rapid (ca. 1 min) lightening of the solution occurred and new IR bands were observed at 2042 vs, 2021 m, and 1988 m cm^{-1}. This species also decomposed slowly, and all attempts to further characterize the product were unsuccessful. For **4** the dark red solution lightened immediately upon addition of acid and new IR bands at 2071 vs, 2015 s, 1984 m, 1954 m, and 1908 w cm^{-1} were observed. These slowly decayed with concomitant decomposition of the product over approximately 3 h. Similar behavior was noted for **5** and **6**, the products being characterized by IR bands at 2100 vs, 2048 s, 1972 m, and 1885 w cm^{-1} and at 2099 vs, 2047 s, 1978 m, and 1880 w cm^{-1}, respectively.

Oxidation. $[Cp_2Fe][PF_6]$ (0.828 mg, 2.5 × 10^{-3} mmol) was dissolved in a minimum amount of CH_2Cl_2, and this solution was then added in the presence of air to a CH_2Cl_2 solution containing 2.5 × 10^{-3} mmol of **1**−**6** prepared as above. The mixture was immediately transferred to an IR cell and monitored over time. For **1** and **2** no significant changes were noted, while for **3**−**6**, IR changes very similar to those noted above resulted, suggesting that the two reactions were generating the same products.

Electrochemistry. Electrochemistry was carried out in deoxygenated dichloromethane or acetonitrile with 0.1 M $TBAPF_6$ as supporting electrolyte. The working electrode was a 3 mm diameter glassy-carbon electrode which was polished with 0.3 μm alumina slurry prior to each scan. The counter electrode was a Pt wire, and the quasi-reference electrode was a silver wire. All CVs were referenced to the Fc/Fc^+ redox couple. An Autolab potentiostat (EcoChemie, The Netherlands) was used for all electrochemical measurements. Catalysis studies were carried out by adding equivalents of $HBF_4{\cdot}Et_2O$ (Sigma-Aldrich).

X-ray Crystallography. Single crystals were mounted on fibers and diffraction data collected at 150 K on a Bruker SMART APEX diffractometer using Mo Kα radiation (λ = 0.71073 Å). Data collection, indexing, and initial cell refinements were all done using SMART software.[56] Data reduction was accomplished with SAINT[57] software, and SADABS[58] programs were used to apply empirical absorption corrections. The structures were solved by direct methods or Patterson methods and refined by full-matrix least squares (SHELXTL, V6.12).[59] All non-hydrogen atoms were refined anisotropically, and hydrogen atoms were included using a riding model. Scattering factors were taken from the International Tables for X-ray Crystallography. The crystal of **3** showed significant decomposition during the data collection. It contained some solvent, which was modeled as a highly disordered molecule of pentane and also a molecule of methanol. The protons on these were not calculated. It is likely that the poor quality of the overall data reflects the partial loss of one or both of these solvents during the experiment. This does not adversely affect the overall structure of the complex but is reflected in the relatively poor esds. Additional details of data collection and structure refinement are given in Table 3.

Computational Methodology. The DFT calculations reported here were performed with the Gaussian09 package of programs.[60] The calculations were carried out with the B3LYP functional, which utilizes the Becke three-parameter exchange functional (B3)[61] combined with the correlation functional of Lee, Yang, and Parr (LYP).[62] The iron and ruthenium atoms were described by Stuttgart−Dresden effective core potentials (ecp) and the SDD basis set, while the 6-31G(d′) basis set, as implemented in the Gaussian09 program suite, was employed for the remaining atoms. The geometry-optimized structures reported here represent minima based on zero imaginary frequencies (positive eigenvalues), as established by frequency calculations using the analytical Hessian. The computed harmonic frequencies for the carbonyl stretching bands have been scaled using Radom's scaling factor of 0.9614.[63] The charges associated with the non-hydrogen atoms in compounds **1**−**4** were determined by natural population analyses (NPA) at the B3LYP level of theory.[64] The geometry-optimized structures have been drawn with the JIMP2 molecular visualization and manipulation program.[65]

■ ASSOCIATED CONTENT

Ⓢ Supporting Information

Text, tables, figures, and CIF files giving details of the X-ray crystallographic structure determinations of **1**−**4**, HOMO and LUMO contour plots of the geometry-optimized structures of clusters **1**−**4** and the geometry-optimized structures of the isomeric clusters $[Ru_3(CO)_7(edt)_2]$, the complete ref 60, atomic coordinates of all optimized stationary points, and additional electrochemical information and experiments (Figures S1−S5). This material is available free of charge via the Internet at http://pubs.acs.org. Crystal data for **1**−**4** are also available from http://www.ccdc.cam.ac.uk/conts/retrieving.html as supplementary publications CCDC 827274−827276 (mail, 12 Union Road, Cambridge CB2 1FZ, U.K.; fax, +44-1223-336033; e-mail, deposit@ccdc.cam.ac.uk).

■ AUTHOR INFORMATION

Corresponding Author

*E-mail: graeme.hogarth@kcl.ac.uk (G.H.); k.b.holt@ucl.ac.uk (K.B.H.); skabir_ju@yahoo.com (S.E.K.).

Notes

The authors declare no competing financial interest.

■ ACKNOWLEDGMENTS

This research has been partially sponsored by the Ministry of Science and Information & Communication Technology, Government of the People's Republic of Bangladesh. We thank University College London for the provision of a studentship (D.U.), the EPSRC for an Advanced Fellowship (K.B.H., Grant No EP/D070538/1), the Commonwealth Scholarship Commission (S.G.) and the European Commission for Erasmus Mundus doctoral (A.R.) and post-doctoral (S.B.M.) fellowships. G.H. thanks The Royal Society of Chemistry for an International Authors Grant, which allowed

this manuscript to be completed during his visit to the University of North Texas. M.G.R. acknowledges support from the Robert A. Welch Foundation (Grant B-1093-MGR) and NSF (CHE-0741936). We also thank Prof. Michael B. Hall (TAMU) for providing us a copy of his JIMP2 program, which was used to prepare the geometry-optimized structures reported here. M.G.R. also thanks Dr. David A. Hrovat (Center for Advanced Scientific Computing and Modeling, UNT) for helpful computational discussions.

REFERENCES

(1) Georgakaki, I. P.; Thomson, L. M.; Lyon, E. J.; Hall, M. B.; Darensbourg, M. Y. *Coord. Chem. Rev.* **2003**, *238*−*239*, 255.
(2) Evans, D. J.; Pickett, C. J. *Chem. Soc. Rev.* **2003**, *32*, 268.
(3) Rauchfuss, T. B. *Inorg. Chem.* **2004**, *43*, 14.
(4) Sun, L.; Åkermark, B.; Ott, S. *Coord. Chem. Rev.* **2005**, *249*, 1653.
(5) Liu, X.; Ibrahim, S. K.; Tard, C.; Pickett, C. J. *Coord. Chem. Rev.* **2005**, *249*, 1641.
(6) Nicolet, Y.; Piras, C.; Legrand, P.; Hatchikian, C. E.; Fontecilla-Camps, J. C. *Structure* **1999**, *7*, 13.
(7) Peters, J. W.; Lanzilotta, W. N.; Lemon, B.; Seefeldt, L. C. *Science* **1998**, *282*, 1853.
(8) Lemon, B. J.; Peters, J. W. *Biochemistry* **1999**, *38*, 12969.
(9) Bruschi, M.; Greco, C.; Kaukonen, M.; Fantucci, P.; Ryde, U.; De Gioia, L. *Angew. Chem., Int. Ed.* **2009**, *48*, 3503.
(10) Greco, C.; Fantucci, P.; De Gioia, L.; Suarez-Bertoa, R.; Bruschi, M.; Talarmin, J.; Schollhammer, P. *Dalton Trans.* **2010**, *39*, 7320.
(11) Greco, C.; Zampella, G.; Bertini, L.; Bruschi, M.; Fantucci, P.; De Gioia, L. *Inorg. Chem.* **2007**, *46*, 108.
(12) Surawatanawong, P.; Tye, J. W.; Darensbourg, M. Y.; Hall, M. B. *Dalton Trans.* **2010**, *39*, 3093.
(13) Tard, C.; Liu, X.; Hughes, D. L.; Pickett, C. J. *Chem. Commun.* **2005**, 133.
(14) Feasey, N. D.; Forrow, N. J.; Hogarth, G.; Knox, S. A. R.; Macpherson, K. A.; Morris, M. J.; Orpen, A. G. *J. Organomet. Chem.* **1984**, *267*, C41.
(15) Polm, L. H.; Mul, W. P.; Elsevier, C. J.; Vrieze, K.; Christophersen, M. J. N.; Stam, C. H. *Organometallics* **1988**, *7*, 423.
(16) Delgado, E.; Chi, Y.; Wang, W.; Hogarth, G.; Low, P. J.; Enright, G. D.; Peng, S.-M.; Lee, G.-H.; Carty, A. J. *Organometallics* **1998**, *17*, 2936.
(17) Bergamo, M.; Beringhelli, T.; D'Alfonso, G.; Mercandelli, P.; Moret, M.; Sironi, A. *Organometallics* **1997**, *16*, 4129.
(18) Tzeng, Y.-F.; Wu, C.-Y.; Hwang, W.-S.; Hung, C.-H. *J. Organomet. Chem.* **2003**, *687*, 16.
(19) Mul, W. P.; Elsevier, C. J.; Van Leijen, M.; Vrieze, K.; Smeets, W. J. J.; Spek, A. L. *Organometallics* **1992**, *11*, 1877.
(20) Cheah, M. H.; Tard, C.; Borg, S. J.; Liu, X.; Ibrahim, S. K.; Pickett, C. J.; Best, S. P. *J. Am. Chem. Soc.* **2007**, *129*, 11085.
(21) Surawatanawong, P.; Hall, M. B. *Inorg. Chem.* **2010**, *49*, 5737.
(22) Winter, A.; Zsolnai, L.; Huttner, G. *Z. Naturforsch., B* **1982**, *37B*, 1430.
(23) Ghosh, S.; Hogarth, G.; Holt, K. B.; Kabir, S. E.; Rahaman, A.; Unwin, D. G. *Chem. Commun.* **2011**, *47*, 11222.
(24) Capon, J.-F.; Gloaguen, F.; Petillon, F. Y.; Schollhammer, P.; Talarmin, J. *Eur. J. Inorg. Chem.* **2008**, 4671.
(25) Lyon, E. J.; Georgakaki, I. P.; Reibenspies, J. H.; Darensbourg, M. Y. *Angew. Chem., Int. Ed.* **1999**, *38*, 3178.
(26) Lyon, E. J.; Georgakaki, I. P.; Reibenspies, J. H.; Darensbourg, M. Y. *J. Am. Chem. Soc.* **2001**, *123*, 3268.
(27) Zhao, X.; Georgakaki, I. P.; Miller, M. L.; Mejia-Rodriguez, R.; Chiang, C.-Y.; Darensbourg, M. Y. *Inorg. Chem.* **2002**, *41*, 3917.
(28) Gloaguen, F.; Lawrence, J. D.; Rauchfuss, T. B.; Bénard, M.; Rohmer, M.-M. *Inorg. Chem.* **2002**, *41*, 6573.
(29) Capon, J.-F.; El Hassnaoui, S.; Gloaguen, F.; Schollhammer, P.; Talarmin, J. *Organometallics* **2005**, *24*, 2020.
(30) Li, P.; Wang, M.; He, C.; Li, G.; Liu, X.; Chen, C.; Åkermark, B.; Sun, L. *Eur. J. Inorg. Chem.* **2005**, *44*, 2506.
(31) Adam, F. I.; Hogarth, G.; Richards, I. *J. Organomet. Chem.* **2007**, *692*, 3957.
(32) Ezzaher, S.; Capon, J.-F.; Gloaguen, F.; Petillon, F. Y.; Schollhammer, P.; Talarmin, J. *Inorg. Chem.* **2007**, *46*, 9863.
(33) Adam, F. I.; Hogarth, G.; Richards, I.; Sanchez, B. E. *Dalton Trans.* **2007**, 2485.
(34) Ezzaher, S.; Capon, J.-F.; Gloaguen, F.; Petillon, F. Y.; Schollhammer, P.; Talarmin, J.; Pichon, R.; Kervarec, N. *Inorg. Chem.* **2007**, *46*, 3426.
(35) Lounissi, S.; Capon, J.-F.; Gloaguen, F.; Matoussi, F.; Petillon, F. Y.; Schollhammer, P.; Talarmin, J. *Chem. Commun.* **2011**, *47*, 878.
(36) Adam, F. I.; Hogarth, G.; Kabir, S. E.; Richards, I. R. *C. R. Chim.* **2008**, *11*, 890.
(37) Justice, A. K.; Zampella, G.; De Gioia, L.; Rauchfuss, T. B.; van der Vlugt, J. I.; Wilson, S. R. *Inorg. Chem.* **2007**, *46*, 1655.
(38) (a) Ellgen, P. C.; Gerlach, J. N. *Inorg. Chem.* **1973**, *12*, 2526. (b) Gregori, G. MSc Thesis, University College London, 2009.
(39) Rahaman, A.; Ghosh, S.; Hollingsworth, N.; Kabir, S. E.; Nordlander, E.; Richmond, M. G.; Hogarth, G. Unpublished results.
(40) Lounissi, S.; Capon, J.-F.; Gloaguen, F.; Matoussi, F.; Pétillon, F. Y.; Schollhammer, P.; Talarmin, J. *Chem. Commun.* **2011**, *47*, 878.
(41) Adams, R. D.; Yamamoto, J. H. *J. Cluster Sci.* **1996**, *7*, 643.
(42) Liu, T.; Darensbourg, M. Y. *J. Am. Chem. Soc.* **2007**, *129*, 7008.
(43) Justice, A. K.; Rauchfuss, T. B.; Wilson, S. R. *Angew. Chem., Int. Ed.* **2007**, *46*, 6152.
(44) Thomas, C. M.; Liu, T.; Hall, M. B.; Darensbourg, M. Y. *Chem. Commun.* **2008**, 1563.
(45) Thomas, C. M.; Darensbourg, M. Y.; Hall, M. B. *J. Inorg. Biochem.* **2007**, *101*, 1752.
(46) Matthews, S. L.; Heinekey, D. M. *Inorg. Chem.* **2010**, *49*, 9746.
(47) Orain, P.-Y.; Capon, J.-F.; Gloaguen, F.; Petillon, F. Y.; Schollhammer, P.; Talarmin, J.; Zampella, G.; De Gioia, L.; Rosinel, T. *Inorg. Chem.* **2010**, *49*, 5003.
(48) Barton, B. E.; Zampella, G.; Justice, A. K.; De Gioia, L.; Rauchfuss, T. B.; Wilson, S. R. *Dalton Trans.* **2010**, *39*, 3011.
(49) Felton, G. A. N.; Petro, B. J.; Glass, R. S.; Lichtenberger, D. L.; Evans, D. H. *J. Am. Chem. Soc.* **2009**, *131*, 11290.
(50) Wang, W.; Nilges, M. J.; Rauchfuss, T. B.; Stein, M. *J. Am. Chem. Soc.* **2013**, *135*, 3633−3639.
(51) Zampella, G.; Greco, C.; Fantucci, P.; De Gioia, L. *Inorg. Chem.* **2006**, *45*, 4109.
(52) Li, Z.; Zeng, X.; Niu, Z.; Liu, X. *Electrochim. Acta* **2009**, *54*, 3638.
(53) Yeo, J.; Cheah, M. H.; Bondin, M. I.; Best, S. P. *Aust. J. Chem.* **2012**, *65*, 241.
(54) Gao, W.; Sun, J.; Li, M.; Åkermark, T.; Romare, K.; Sun, L.; Åkermark, B. *Eur. J. Inorg. Chem.* **2011**, 1100.
(55) Mebi, C. A.; Brigance, K. E.; Bowman, R. B. *J. Braz. Chem. Soc.* **2012**, *23*, 186.
(56) *SMART Version 5.628*; Bruker AXS, Inc., 5465 East Cheryl Parkway, Madison, WI 53711-5373, 2003.
(57) *SAINT Version 6.36A*; Bruker AXS, Inc., 5465 East Cheryl Parkway, Madison, WI 53711-5373, 2002.
(58) Sheldrick, G. M. *SADABS Version 2.10*; University of Göttingen, Göttingen, Germany, 2003.
(59) Sheldrick, G. M. A short history of SHELX. *Acta Crystallogr.* **2008**, *A64*, 112.
(60) Frisch, M. J., et al. *Gaussian 09, Revision E.01*; Gaussian, Inc., Wallingford, CT, USA, 2009.
(61) Becke, A. D. *J. Chem. Phys.* **1993**, *98*, 5648.
(62) Lee, C.; Yang, W.; Parr, R. G. *Phys. Rev. B* **1993**, *37*, 785.
(63) Scott, A. P.; Radom, L. *J. Phys. Chem.* **1996**, *100*, 16502.
(64) Reed, A. E.; Curtiss, L. A.; Weinhold, F. *Chem. Rev.* **1988**, *88*, 899.
(65) (a) JIMP2, version 0.091, a free program for the visualization and manipulation of molecules: Hall, M. B.; Fenske, R. F. *Inorg. Chem.* **1972**, *11*, 768. (b) Manson, J.; Webster, C. E.; Hall, M. B. Texas A&M University, College Station, TX, 2006; http://www.chem.tamu.edu/jimp2/index.html.